Lifetime measurement of the 59.54-keV state in ^{237}Np

L. J. Sun[1],[*] J. Dopfer[2,1], A. Adams[2,1], and C. Wrede[2,1][†]

[1] Facility for Rare Isotope Beams, Michigan State University, East Lansing, Michigan 48824, USA
[2] Department of Physics and Astronomy, Michigan State University, East Lansing, Michigan 48824, USA

(Dated: February 3, 2025)

The α-γ coincidence of ^{241}Am has been measured using the Si and Ge detectors that are part of the Lifetimes and Branching Ratios Apparatus. A new half-life value for the 59.54-keV isomeric state in ^{237}Np has been determined using Bayesian analysis with rigorous uncertainty quantification. Furthermore, a comprehensive reevaluation of all available data has been performed. The implications of our results extend to a discussion of the Mössbauer effect.

I. INTRODUCTION

II. EXPERIMENTAL SETUP

We have developed the Lifetimes and Branching Ratios Apparatus (LIBRA) [1] to be used in the stopped-beam area at the Facility for Rare Isotope Beams. This apparatus is designed to measure the decay branching ratios of resonances populated by electron capture and β^+ decay, as well as to measure lifetimes in the $10^{-17} - 10^{-15}$ s range for resonances populated by electron capture using the Particle X-ray Coincidence Technique (PXCT) [2].

A disc-shaped Low Energy Germanium detector (LEGe), Mirion GL0510 [3], is used to detect X rays and low-energy γ rays. The LEGe detector comprises a Ge crystal with a diameter of 25.0 mm and a thickness of 10.5 mm. Two single-sided, single-area circular Si detectors, Micron MSD12 and MSD26, are used to detect charged particles. The active volume of MSD12 is 12 μm in thickness and 12 mm in diameter [4], and MSD26 is 1000 μm thick and 26 mm in diameter [5].

The signals from each preamplifier are digitized by a 16-bit, 250 MHz XIA Pixie-16 module [6, 7]. The Digital Data Acquisition System (DDAS) [8, 9] is used for recording and processing data. Trapezoidal filtering algorithms are implemented in both the slow filter for pulse amplitude measurement and the fast filter for leading-edge triggering. Each event is timestamped using a Constant Fraction Discriminator (CFD) algorithm based on the trigger filter response.

An ^{241}Am source of 3.44×10^3 Bq with an active area 3 mm in diameter is installed roughly at the center of the chamber. The source faces the MSD with an Al aperture installed in between, and its substrate is 127-μm-thick Pt.
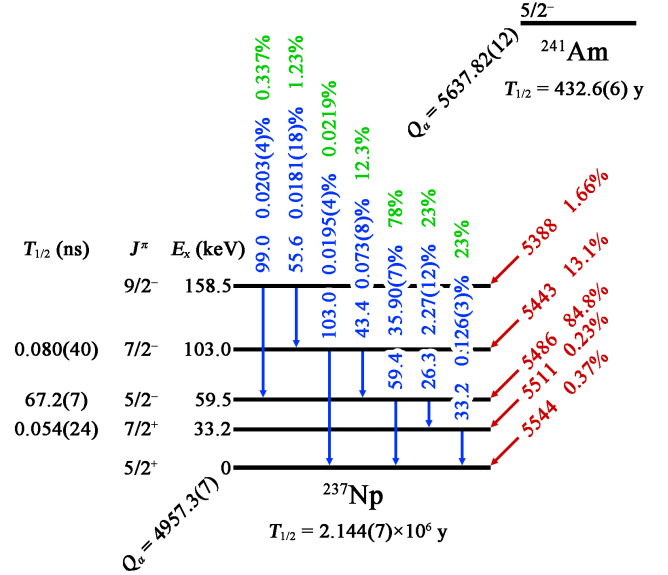
Table II summarizes the conditions of the measurements.

FIG. 1. Simplified decay scheme of ^{241}Am. All energy, half-life, spin, and parity values are adopted from Ref. [12]. The α transitions are labeled with their kinetic energies in keV and absolute intensities per ^{241}Am decay. The deexcitations of ^{237}Np states are labeled with their γ-ray energies and absolute intensities of emitted photons, followed by total transition intensities taking into account internal conversion coefficients [12].

III. LIFETIME ANALYSIS

Figure 4 shows the α-γ coincidence spectra between MSD and LEGe. The of substrate ^{241}Am source attenuates most of the low-energy photons emitted towards LEGe, leaving mainly the 59.5-keV ^{237}Np γ ray and its escape peaks observable.

Figure 6 shows the α-γ time difference distribution constructed by the start timestamps from 5486-keV α measured by MSD and the stop timestamps from the 59.5-keV γ ray deexciting the 59.5-keV state in ^{237}Np measured by LEGe. By fitting the time spectra with a function

TABLE I. Settings of measurements.

	Run 1	Run 2	Run 3
Measurement Date	$10/30/2023-12/12/2023$	$12/20/2023-2/17/2024$	$5/22/2024-5/30/2024$
Measurement Time (h)	949.2	1043.7	185.0
Detectors	MSD12+MSD26	MSD26	MSD12+MSD26
Collimator Diameter (mm)	5	2	5
MSD12 Trigger T_{Rise} (μs)	0.112	0.112	0.016
MSD12 Trigger T_{Gap} (μs)	0.304	0.304	1.000
MSD26 Trigger T_{Rise} (μs)	0.248	0.248	0.016
MSD26 Trigger T_{Gap} (μs)	0.200	0.200	1.000
LEGe Trigger T_{Rise} (μs)	0.200	0.200	0.064
LEGe Trigger T_{Gap} (μs)	0.104	0.104	0.952
CFD Delay (μs)	0.304	0.304	0.304
CFD Scale (μs)	0	0	7
Event-build Window (μs)	± 1.5	± 1.5	± 1.5
MSD12 Count Rate (s^{-1})	145	$-$	180
MSD26 Count Rate (s^{-1})	159	32	191
LEGe Count Rate (s^{-1})	37	37	34
α-energy Gate	$5317-5517$	$5459-5499$	$5317-5517$
X-ray-energy Gate	$59.0-60.1$	$59.0-60.1$	$59.0-60.1$
$T_{1/2}$ by LEGe$-$MSD12	68.12 ± 0.13	$-$	67.77 ± 0.25
$T_{1/2}$ by LEGe$-$MSD26	68.06 ± 0.07	67.91 ± 0.20	67.88 ± 0.20

TABLE II. ^{241}Am main α decay branches and effective energy loss in detectors.

		Run 1 and Run 3			Run 2
I_α (%)	E_α (keV)	ΔE (keV)	E_r (keV)	E_{tot} (keV)	E_{tot} (keV)
84.8(5)	5486	1791	3626	5417	5479
13.1(3)	5443	1803	3571	5374	5436
1.66(2)	5388	1818	3501	5319	5381

FIG. 3. ^{241}Am X-ray and γ-ray energy spectra measured by LEGe. X-ray energy values are adopted from Ref. [11] rounded to the nearest 0.01 keV. γ-ray energy values are adopted from Ref. [12] rounded to the nearest 0.01 keV.
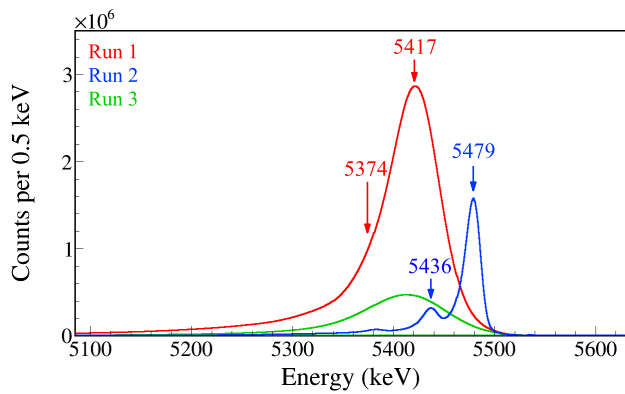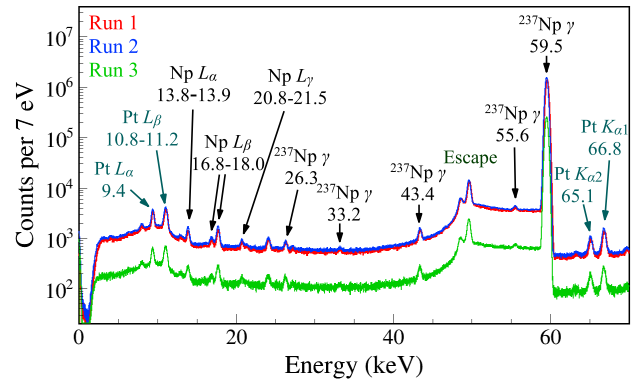

FIG. 2. Red/Green: ^{241}Am α-energy spectra measured by summing MSD12 (energy-loss) and MSD26 (residual energy). The primary peak is at 5417 keV with the minor peak at 5374 keV submerged in the low-energy tail. Blue: ^{241}Am α-energy spectrum measured by MSD26 alone. The primary peak is at 5479 keV and the minor peak is at 5436 keV.

FIG. 4. α-γ coincidence spectra between the MSD and LEGe obtained using the ^{241}Am source placed at the center of the chamber. Only MSD26 is used in Run 2 (middle panel).
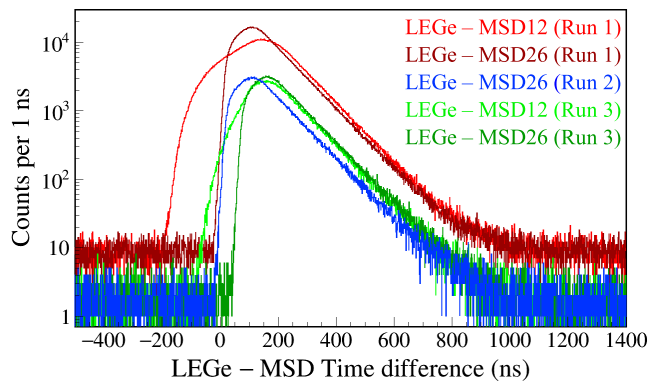
FIG. 5. Time differences between the 59.5-keV γ-ray signals in LEGe and the 5486-keV α signals in MSD. For Run 1 and Run 3, an α gate of 5417 ± 60 keV is set on the MSD sum energy. For Run 2, an α gate of 5479 ± 20 keV is set on the energy measured by MSD26 alone.

$$f_{\text{direct}}(t; N_{59}, T_{59}, B) = \frac{N_{59}\ln(2)}{T_{59}} \exp\left[-\frac{t\ln(2)}{T_{59}}\right] + B \tag{1}$$

composed of the total number of decays (N_{59}), the exponential decay half-life (T_{59}), and a constant background (B), we obtained the half-life of the 59.5-keV excited state in ^{237}Np to be 68.1(6) ns (MSD12) and 67.9(5) ns (MSD26), respectively. The results obtained from both Si detectors are consistent with recent precision measurements of 67.86(9) ns [13] and 67.60(25) ns [14].

The 5443-keV α decay populates the 103-keV excited state in ^{237}Np, and then predominantly populates the 59-keV state by internal conversion. As the α gate for the 5486-keV peak for Run 1 and Run 3 also contains the 5443-keV peak, both 5486-59 direct feeding and 5443-103-59 indirect feeding should be taken into account.

$$f_{\text{cascade}}(t; N_{59}, T_{59}, T_{103}, k, B) =$$
$$\frac{N_{59}\ln(2)}{T_{59}} \exp\left[-\frac{t\ln(2)}{T_{59}}\right]$$
$$+ k \cdot N_{59} \cdot \frac{\ln(2)}{T_{103}} \cdot \frac{\ln(2)}{T_{59}} \cdot \frac{\exp\left[\frac{-t\ln(2)}{T_{103}}\right] - \exp\left[\frac{-t\ln(2)}{T_{59}}\right]}{\frac{\ln(2)}{T_{59}} - \frac{\ln(2)}{T_{103}}}$$
$$+ B \tag{2}$$

Figure 6 shows the α-γ time difference distribution constructed by the start timestamps from 5486-keV α measured by the two MSDs and the stop timestamps from the 59.5-keV γ ray deexciting the 59.5-keV state in ^{237}Np measured by LEGe. By fitting the distribution with a function composed of the total number of decays (N), the half-life of exponential decay (T), and a constant

background (B), we obtained the half-life of the 59.5-keV excited state in ^{237}Np to be 68.08(9) ns (MSD12) and 68.01(7) ns (MSD26), respectively. The fit was conducted using the Bayesian method with the affine-invariant ensemble sampler for Markov chain Monte Carlo (MCMC) in the emcee package [16]. The MCMC was run with 100 walkers taking 10,000 steps, giving a total of 10^6 samples. The posterior results obtained from the MCMC sampling are demonstrated in Fig. 7. The half-life value and its 1σ uncertainties are determined by extracting the 16th, 50th, and 84th percentile values from the marginalized posterior distribution. The results obtained from both Si detectors are consistent with recent precision measurements of 67.86(9) ns [13] and 67.60(25) ns [14]. Two factors limit the time resolution that can be achieved with semiconductor detectors. Firstly, the charge collection process is inherently slow, typically taking several hundred nanoseconds. This timescale is much longer than the output from scintillators, making it hard to achieve the same level of timing performance. Secondly, the pulse rise shape from semiconductor detectors can vary significantly from event to event, resulting in a larger uncertainty in generating timestamps.
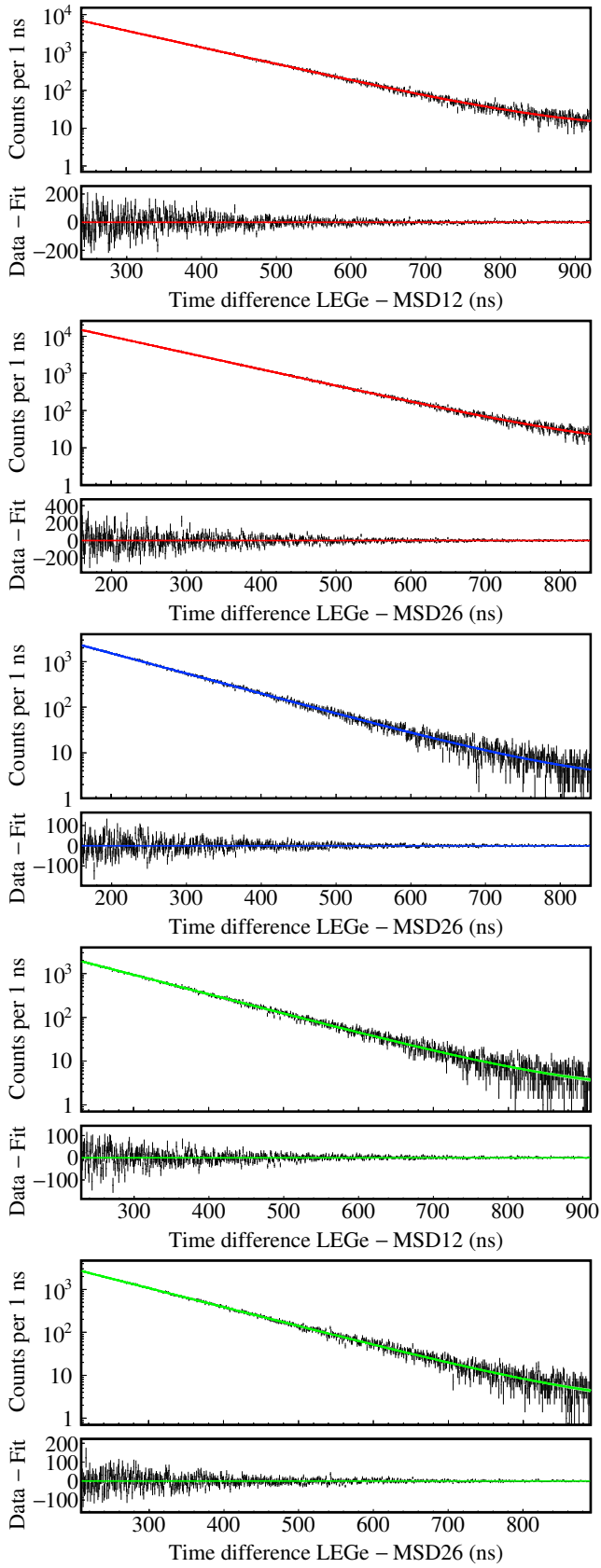
FIG. 6. Time differences between the 59.5-keV γ-ray signals in LEGe and the 5486-keV α signals in MSD. The fit curves in red, blue, and green represent Run 1, Run 2, and Run 3, respectively.
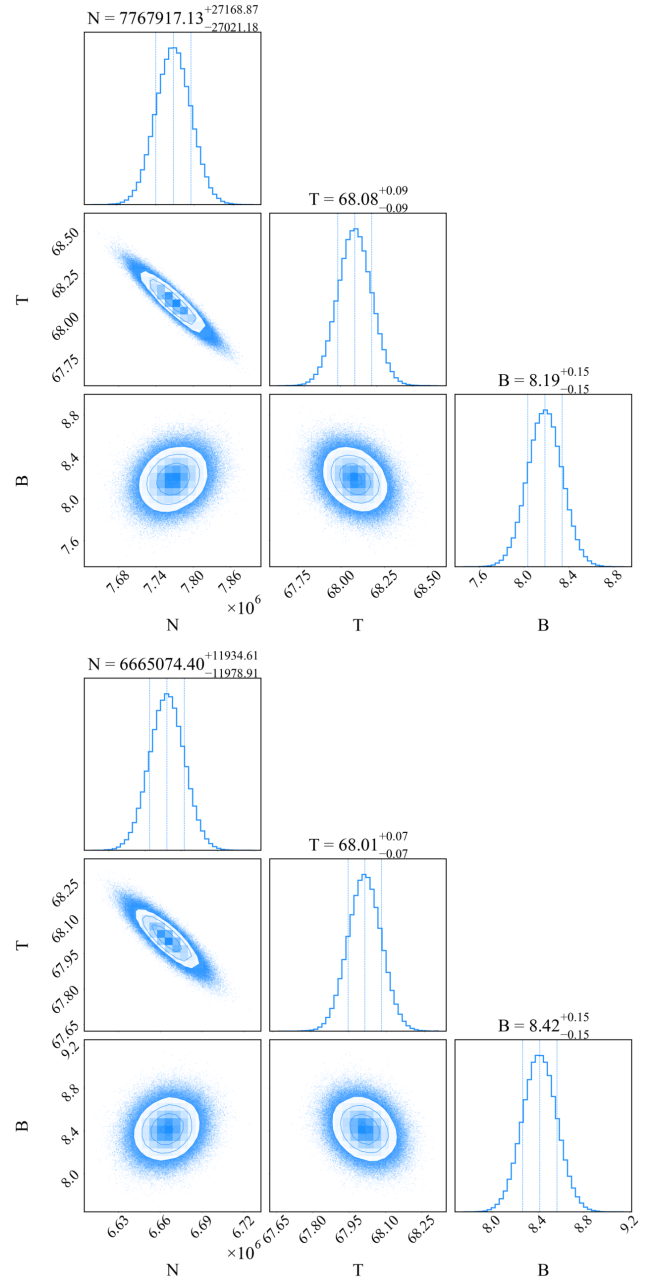

FIG. 7. Posterior distributions of the decay fit parameters. Upper: MSD12. Lower: MSD26. (placeholder)

IV. SUMMARY & OUTLOOK

V. ACKNOWLEDGMENTS

[1] L. J. Sun, J. Dopfer, A. Adams, C. Wrede, A. Banerjee, B. A. Brown, J. Chen, E. A. M. Jensen, R. Mahajan, T. Rauscher, C. Sumithrarachchi, L. E. Weghorn, D. Weisshaar, and T. Wheeler, submitted to Phys. Rev. C. (arXiv:2410.16446.)

[2] J. C. Hardy, J. A. Macdonald, H. Schmeing, H. R. Andrews, J. S. Geiger, R. L. Graham, T. Faestermann, E. T. H. Clifford, and K. P. Jackson, Phys. Rev. Lett. 37, 133 (1976).

[3] MIRION Low Energy Germanium Detector.

[4] MIRCON MSD12 Circular Silicon Detector.

[5] MIRCON MSD26 Circular Silicon Detector.

[6] XIA Pixie-16 Digitizer.

[7] XIA Pixie-16 Digitizer User Manual.

[8] K. Starosta, C. Vaman, D. Miller, P. Voss, D. Bazin, T. Glasmacher, H. Crawford, P. Mantica, H. Tan, W. Hennig, M. Walby, A. Fallu-Labruyere, J. Harris, D. Breus, P. Grudberg, W.K. Warburton, Nucl. Instrum. Methods Phys. Res. A 610, 700 (2009).

[9] C.J. Prokop, S.N. Liddick, B.L. Abromeit, A.T. Chemey, N.R. Larson, S. Suchyta, J.R. Tompkins, Nucl. Instrum. Methods Phys. Res. A 741, 163 (2014).

[10] M.-M. Bé, V. Chisté, C. Dulieu, X. Mougeot, E. Browne, V. Chechev, N. Kuzmenko, F. Kondev, A. Luca, M. Galán, A.L. Nichols, A. Arinc, and X. Huang, Mono. BIPM-5 - Table of Radionuclides, Vol.5 (2010).

[11] Matt Newville, easyXAFS, Matteo Levantino, Christian Schlepuetz, Damian Günzing, Max Rakitin, Sang-Woo Kim, and kalvdans, xraypy/XrayDB: (4.5.1). Zenodo (2023).

[12] M. Basunia, Nucl. Data Sheets 107, 2323 (2006).

[13] Marcell P. Takács, Karsten Kossert, Appl. Radiat. Isot. 176, 109858 (2021).

[14] Chavdar Dutsov, Benoît Sabot, Philippe Cassette, Krasimir Mitev, Appl. Radiat. Isot. 176, 109845 (2021).

[15] O. C. B. Santos, J. R. B. Oliveira, E. Macchione, R. Lichtenthäler, K. C. C. Pires, A. Lépine-Szily, Nucl. Phys. A 1040, 122745 (2023).

[16] D. Foreman-Mackey, D. W. Hogg, D. Lang, and J. Goodman, Publ. Astron. Soc. Pac. 125, 306 (2013).

[17] M. Vretenar, N. Erceg, and M. Karuza, Am. J. Phys. 87, 997 (2019).

[18] W.-J. Ong, H. Schatz, K. Kravvaris, S. Ahn, K. Childers, B. P. Crider, A. C. Dombos, C. Langer, R. Lewis, S. N. Liddick, S. Lyons, Z. Meisel, F. Montes, J. Pereira, D. Richman, K. Schmidt, and A. Spyrou, Phys. Rev. C 110, 024321 (2024).